ARCHIVES OF ELECTRICAL ENGINEERING VOL. 69(3), pp. 705–721 (2020)

DOI 10.24425/aee.2020.133927

Improvement of damping characteristics and index evaluation of a wind-PV-thermal-bundled power transmission system by combining PSS and SSSC

PING HE, XINXIN WU, CONGSHAN LI, MINGMING ZHENG, ZHAO LI

Zhengzhou University of Light Industry
No.5, Dongfeng Road, Jinshui District, Zhengzhou City, Henan Province, China, 450002
e-mail: hplkz@126.com

(Received: 16.12.2019, revised: 29.04.2020)

Abstract: The grid integration of large-scale wind and solar energy affects the power flow of wind-PV-thermal-bundled power transmission systems and may introduce an unpredicted threat to the power system's small signal stability. Meanwhile, a power system stabilizer (PSS) and static synchronous series compensator (SSSC) play an important role in improving the static and dynamic stability of the system. Based on this scenario and in view of the actual engineering requirements, the framework of wind-PV-thermal-bundled power transmitted by an AC/DC system with the PSS and SSSC is established considering the fluctuation of wind and photovoltaic power output and the characteristics of the PSS and SSSC. Afterwards, the situation model is constructed in the IEEE 2-area 4-unit system, and the influence of the PSS and SSSC on the system stability under different operating conditions is analyzed in detail through eigenvalue analysis and time-domain simulation. Finally, an index named the gain rate is defined to describe the improvement of the stability limitations of various wind-PV-thermal operating conditions with the PSS and SSSC. The results indicate (K) that the damping characteristics, dynamic stability and stability limitations for various wind-PV-thermal operating conditions of the wind-PV-thermal-bundled power transmission system can be significantly improved by the interaction of the PSS and SSSC.

Key words: damping characteristics, eigenvalue analysis, power system stabilizer, wind-PV-thermal-bundled power system

1. Introduction

With the advantages of mitigating energy crises and protecting the environment [1], wind-PV-thermal-bundled power transmitted by AC/DC systems is widely applied in the new energy

delivery for large-scale energy bases in northwest, north, and northeast China. This can not only promote the comprehensive development and utilization of new energy bases and greatly alleviate the problem of electricity shortages in the central and eastern regions of China but also suppress peak shaving changes caused by fluctuations of wind and solar energy and improve the stability of long-distance power transmission and the utilization of DC equipment [2]. In this scenario, the large-scale integration of wind and solar energy, however, will also bring about adverse effects on power systems. Doubly fed induction generators (DFIGs) and photovoltaic power stations, associated with wind power and solar power, introduce interactions with synchronous generators (SGs), change the system's power flow and affect the system's damping characteristics, making the power system extremely vulnerable to low frequency oscillations when disturbed due to a decrease of damping [3, 4].The possibility of unbalanced power flow in power systems will markedly increase due to the random fluctuations of wind power [5–8] and photovoltaic power [9–12], introducing new challenges. Therefore, it is of great urgency to apply damping controllers to improve the damping characteristics of wind-PV-thermal-bundled power transmission systems.

Some researchers have drawn much attention to this important topic. The damping of low frequency oscillations, particularly local area oscillations, can be dramatically improved due to the function of a power system stabilizer (PSS) [13–15]; hence, the small signal stability of the system is strengthened. The integration of wind power and photovoltaic power obviously widens the system eigenvalue range, which makes it fairly difficult to improve the small signal stability of inter-region oscillations only using the PSS [16, 17]. In addition, references [18–20] note that flexible AC transmission system (FACTS) devices can not only strengthen the system stability and reliability but also enhance the utilization efficiency of renewable resources by constantly controlling the power flow of transmission lines. The simulation curve of [21] indicates that a static synchronous series compensator (SSSC), as a series FACTS device, can reduce the system oscillation amplitude and accelerate the convergence process. Much work in references [22, 23] has proven that significant improvements in the damping characteristics, synchronous transmission power and transient stability limit can be achieved when using the SSSC. Specifically, as stated in [24], on the one hand, the PSS increases the damping of system oscillations; on the other hand, however, it leads to instability of the torsional mode. In addition, the PSS can be applied in a system with the SSSC with no detrimental influence on the torsional mode.

In this paper, the effects of interactions between the PSS and SSSC on the damping characteristics and dynamic stability of a wind-PV-thermal-bundled power transmission system, including the wind-PV-thermal transmission distance, wind-PV-thermal grid-connect capacity and AC/DC transmission power ratio, are studied. Moreover, the gain rate index (K) is defined to measure the improvement of the stability limitations, which shows how and why the PSS and SSSC can affect the power system small signal stability under various wind-PV-thermal operating conditions. The contributions of the paper to the research field are as follows:

– Establishing the framework of wind-PV-thermal-bundled power transmitted by an AC/DC system with the PSS and SSSC considering the fluctuation of wind and photovoltaic power output and the characteristics of the PSS and SSSC.
– Constructing the situation model in the IEEE 2-area 4-unit system, and analyzing the influence of the PSS and SSSC on the system stability under different operating conditions in detail through eigenvalue analysis and time-domain simulation.

– Defining the gain rate index to measure the improvement of the stability limitations of various wind-PV-thermal operating conditions with the PSS and SSSC.

The main structure of this paper is as follows. Section 1 introduces the research background and purpose of this paper. In Section 2, wind-PV-thermal-bundled power transmission system models are presented, including the wind power unit model, photovoltaic power station model and thermal power unit model. The PSS and SSSC models and basic principles are discussed in Section 3. To study the influence of the PSS and SSSC on the system stability under different operating conditions, case studies are presented in Section 4. The gain rate index (K), defined to measure the improvement of the stability limitations, is discussed in Section 5. Some conclusions are drawn in Section 6.

2. Wind-PV-thermal-bundled power transmission system model

2.1. Thermal power unit model

The simplified synchronous unit model, including the generator equation and rotor motion equation, is used to replace the thermal power unit model.

$$\begin{cases} u_d = E'_d + X'_q i_q - r_a i_d \\ u_q = E'_q + X'_d i_d - r_a i_q \\ T'_{d0} \dfrac{\mathrm{d}E'_q}{\mathrm{d}t} = E_f - E'_q - \left(X_d - X'_d\right) i_d \\ T'_{q0} \dfrac{\mathrm{d}E'_d}{\mathrm{d}t} = -E'_d + \left(X_q - X'_q\right) i_q \\ T_j \dfrac{\mathrm{d}\omega_s}{\mathrm{d}t} + D\left(\omega_s - 1\right) = T_m - \left[E'_q i_q + E'_d i_d - \left(X'_d - X'_q\right) i_d i_q\right] \\ \dfrac{\mathrm{d}\delta}{\mathrm{d}t} = \omega_s - 1 \end{cases}, \tag{1}$$

where: u_d and u_q are the voltage components along the d and q axes; E'_d and E'_q are the transient voltage components along the d and q axes; X_d and X_q are the synchronous reactance components along the d and q axes; X'_d and X'_q are the transient reactance components along the d and q axes; i_d and i_q are the current components along the d and q axes; r_a is the stator winding resistance; T'_{d0} and T'_{q0} are the open-circuit transient time constants; E_f is the stator excitation electromotive force; T_J is the inertial time constant of the generators; T_m is the mechanical torque; ω_s is the angular speed of the synchronous rotor; $D(\omega_s - 1)$ is the equivalent damping; D is the constant damping coefficient; δ is the electrical angle between the generator rotor q axis and system reference axis rotating at the synchronous speed.

2.2. Wind power unit model

Doubly fed induction generators (DFIGs) are currently the most widely used generators in the wind power industry. Considering its good performance, a DFIG is selected as the wind power unit model here.

The aerodynamic mathematical model of wind power units can be described as:

$$P_{mech} = \rho C_p(\lambda\beta)\pi R^2 v^3/2, \tag{2}$$

$$\lambda = \omega R/v, \tag{3}$$

where: P_{mech} is the mechanical power of the wind turbine; ρ is the air density; R is the radius of the impeller of the wind turbine, v is the wind speed; ω is the speed of the wind turbine; λ is the tip speed ratio; β is the pitch angle; and C_p is the wind energy conversion efficiency coefficient of the blade, which is a function of λ and β.

2.3. Photovoltaic power station model

Based on the characteristics of PV cells, the $U - I$ output equation of the photovoltaic array can be described as [25, 26]:

$$I = n_p I_{ph} - n_p I_0 \left(e^{\frac{q(U+IR_S)}{n_S nkT}} - 1\right), \tag{4}$$

where: I and U are the output current and voltage of the photovoltaic array, respectively; n_p and n_s are the numbers of parallel and series modules of the photovoltaic array, respectively; I_{ph} is the photocurrent; I_0 is the reverse saturation current of the diode; R_s is the series resistance of the photovoltaic module; q is the electronic charge; n is the ideal factor of the photovoltaic cell; k is Boltzmann's constant; and T is the absolute temperature.

2.4. High voltage direct current model

The quasi-steady-state model is selected here since it can accurately demonstrate the performance of the high voltage direct current (HVDC)system, which can be expressed as:

$$\begin{cases} I_{dr}^{\&} = \dfrac{1}{L_{dr\Sigma}}\left(-R_d I_{dr} - U_C + \dfrac{3\sqrt{2}}{\pi}U_{dr}\cos\alpha - \dfrac{3}{\pi}X_r I_{dr}\right) \\ I_{di}^{\&} = \dfrac{1}{L_{di\Sigma}}\left(-R_d I_{di} + U_C - \dfrac{3\sqrt{2}}{\pi}U_{di}\cos\varphi - \dfrac{3}{\pi}X_i I_{di}\right) \\ U_C^{\&} = \dfrac{1}{C}(I_{dr} - I_{di}) \end{cases}, \tag{5}$$

where: $I_{dr}^{\&}$, $I_{di}^{\&}$, I_{dr}, I_{di} are the vector and scalar DC current of the rectifier side and inverter side; $U_C^{\&}$, U_C are the vector and scalar midpoint voltage of the DC line; C is the equivalent capacitance of the DC line; R_d is the DC resistance; U_{dr} and U_{di} represent the voltage of the rectifier side and inverter side; X_r and X_i represent the commutation reactance of the rectifier side and inverter side; $L_{dr\Sigma}$ and $L_{di\Sigma}$ represent the equivalent inductance of the rectifier side and inverter side; α is the gating delay angle of the rectifier side; φ is the gating advance angle of the inverter side.

2.5. Wind-PV-thermal-bundled power transmission system model

The wind-PV-thermal-bundled power transmission system consists of large-scale thermal power units, wind power units and photovoltaic power stations, which are connected to the

receiving terminal infinite-bus system via AC/DC transmission lines. The structure diagram of the wind-PV-thermal-bundled power transmission system is shown in Fig. 1.

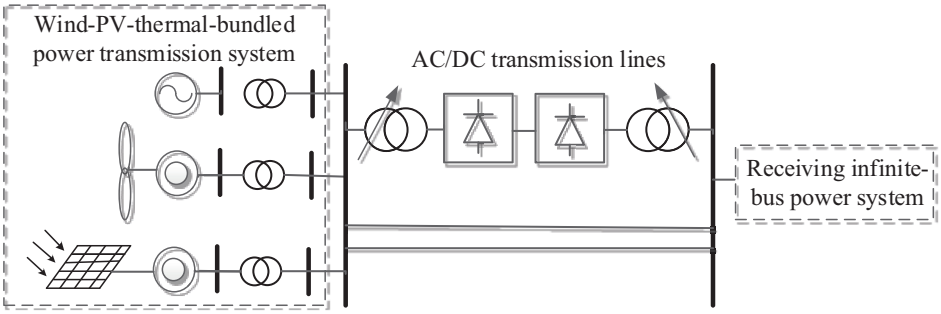

Fig. 1. Structure diagram of the wind-PV-thermal-bundled power transmission system

3. PSS and SSSC model

3.1. PSS model

A PSS is a typical additional excitation control that regulates the active power of the interconnected systems by providing an additional excitation signal to the excitation system and a positive damping to the generator rotor to suppress the low frequency oscillations and enhance the static and dynamic stability of the system [27, 28]. The structure diagram of the PSS is shown in Fig. 2.

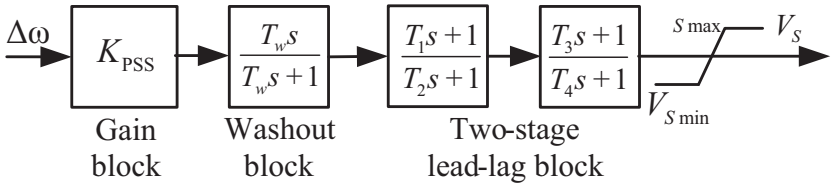

Fig. 2. Structure diagram of PSS

Generally, the PSS is composed of a gain block, a washout block and a two-stage lead-lag block. $\Delta\omega$ is the input speed signal; K_{PSS} is the amplified gain; T_w is the time constant of washout block and normally ranges from 1 to 20 s; $V_{S\,max}$ and $V_{S\,min}$ represent the maximum and minimum output voltage, respectively. Only working in the situation that the output voltage V_S dynamically changes, is the PSS applied as a high-pass filter to effectively clean the interference signal. The two-stage lead-lag block, with time constants T_1, T_2, T_3 and T_4, provides an appropriate specified phase lead to compensate for the phase lag between the input of the excitation system and the electromagnetic torque of the generator.

Based on the structure diagram, the transfer function of a typical PSS is described as:

$$G(s) = K_{PSS}\frac{sT_w}{1+sT_w}\frac{1+sT_1}{1+sT_2}\frac{1+sT_3}{1+sT_4}. \tag{6}$$

3.2. SSSC model

As a series FACTS device, a SSSC consists of a voltage converter, a coupled converter, a DC link and a control system. It can inject a voltage perpendicular to the original current of the line and change the transmission line equivalent impedance to adjust the transmission power and improve the dynamic performance of the power system [29, 30]. The structure diagram of the SSSC is shown in Fig. 3.

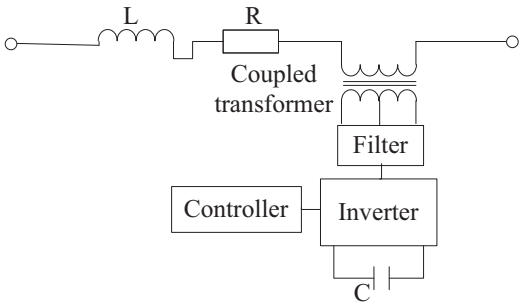

Fig. 3. Structure diagram of SSSC

The mathematical model of the SSSC in $d-q$ axis coordinates is expressed as:

$$\begin{cases} \dfrac{\mathrm{d}i_d}{\mathrm{d}t} = -\dfrac{R}{L}i_d + \omega i_q + \dfrac{1}{L}(u_{sd} - u_{rd} + u_{scd}) \\ \dfrac{\mathrm{d}i_q}{\mathrm{d}t} = -\dfrac{R}{L}i_q + \omega i_d + \dfrac{1}{L}(u_{sq} - u_{rq} + u_{scq}) \\ \dfrac{\mathrm{d}V_{dc}}{\mathrm{d}t} = \dfrac{3(u_{scd}i_d + u_{scq}i_q)}{2V_{dc}C} - \dfrac{V_{dc}}{CR_{dc}} \end{cases}, \tag{7}$$

where: i_d and i_q are the components of the transmission line current along the d and q axes; R and L are the equivalent resistance and inductance on the AC side; ω is the angular speed of the synchronous rotor; u_{sd} and u_{sq} are the components of the sending end voltage along the d and q axes; u_{rd} and u_{rq} are the components of the receiving end voltage along the d and q axes; V_{dc} is the DC voltage; u_{scd} and u_{scq} are the components of the output voltage of the SSSC; C is the capacity; and R_{dc} is the equivalent resistance on the DC side.

4. Effect of PSS and SSSC under various wind-PV-thermal operating conditions

4.1. Simulation model

The simulation model of the wind-PV-thermal-bundled power transmission system with the PSS and SSSC is built under MATLAB/Simulink as shown in Fig. 4. The system consists of the sending system and the receiving system, which are tightly connected by AC and DC transmission

lines. The AC and DC transmission lines extend up to 200 km. The utilization of the DC link has a positive impact on the long distance transmission power system. On the one hand, the power modulation of the DC system can improve the damping of the power system, restrain the low-frequency oscillation, and enhance the transmission capacity of parallel AC transmission lines. On the other hand, properly increasing the power of the DC transmission line and reducing the power of the AC tie-line can improve the total input power of the receiving power grid.

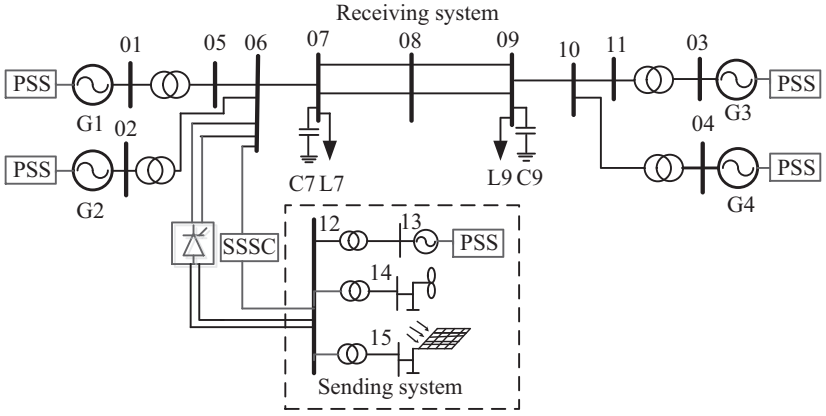

Fig. 4. Simulation model of the wind-PV-thermal-bundled power transmission system

The sending system is a wind-PV-thermal-bundled power transmission system, including thermal power units, wind power units and photovoltaic power stations. The receiving system consists of four generators with the same capacity and the voltage level of 700 MVA/20 kV, which constitute the IEEE 2-area 4-unit system. The PSS is inserted into the excitation system of the thermal power unit, while the SSSC is connected in series to the AC transmission line.

4.2. Effect of transmission distance of wind-PV-thermal-bundled power

To study the influence of a PSS and SSSC on the damping characteristics for a set transmission distance (the distance between bus 6 and bus 12 in Fig. 4) in the wind-PV-thermal-bundled power transmission system, eigenvalue analysis and dynamic time-domain simulation are mainly adopted in this section to study the following three operating conditions when the transmission distance is 200 km:

Case 1: without PSS or SSSC,

Case 2: with PSS only,

Case 3: with PSS and SSSC.

The parameters of the PSS and SSSC are shown in Table 1 and Table 2, respectively.

There are 58 eigenvalues of the test system. Among them, there are indeed several local eigenvalues related to a DFIG and they are not listed in this paper because of their large damping and high stability. Three principles are considered in the selection of eigenvalues. First, the related units. Second, the small or critical damping ratio. Third, the range of frequency.

Partial eigenvalues based on the above three operating conditions are shown in Table 3. The system has five oscillation modes: mode 1 and mode 2 are both local oscillations of the generators

Table 1. Parameters of PSS

Input	K_{PSS}	T_w [s]	T_1 [s]	T_2 [s]	T_3 [s]	T_4 [s]	$V_{S\,max}$	$V_{S\,min}$
$\Delta\omega$	20	10	0.05	0.02	3.0	5.4	0.1	−0.1

Table 2. Parameters of SSSC

Operation mode	Series compensation C_p [%]	Regulator time constant T_r [s]	Max voltage	Min voltage
Constant voltage	53.75	0.005	0.6	−0.6

in the sending system or receiving system; mode 3, mode 4 and mode 5 are the inter-area oscillations between the generators in the sending system and receiving system. As is apparent from Table 1, when the damping device is not added, the damping ratios of case 1 are relatively small. Subsequently, the damping ratios of case 2 all rise dramatically when only the PSS is integrated. In addition, the system has the highest damping ratios in case 3 when the PSS and SSSC are both integrated into the system. Therefore, a conclusion can be drawn that combining the PSS and SSSC gives better damping characteristics than using the PSS alone.

Table 3. Partial eigenvalues of the system when the transmission distance is 200 km

Case	Mode	Eigenvalue (λ)	Damping ratio (ζ) [%]	Related units
Case 1	1	–0.8426 ± j5.9000	14.14	G1 G2
	2	–1.2954 ± j7.1348	17.86	G3 G4
	3	–0.4194 ± j4.9556	10.54	G2 G5
	4	–0.3192 ± j3.0920	10.27	G3–G5
	5	–0.3349 ± j1.0102	31.47	G1–G5, DFIG, PV
Case 2	1	–1.9852 ± j6.1109	30.90	G1 G2
	2	–3.2992 ± j8.8681	34.87	G3 G4
	3	–0.8642 ± j3.7580	22.41	G2 G5
	4	–0.3157 ± j2.8693	10.94	G3–G5
	5	–0.5652 ± j0.9710	50.31	G1–G5, DFIG, PV
Case 3	1	–2.1296 ± j6.2233	32.38	G1 G2
	2	–3.3687 ± j8.8203	35.68	G3 G4
	3	–0.9283 ± j3.9467	22.90	G2 G5
	4	–0.6099 ± j2.9208	20.44	G3-G5
	5	–0.5383 ± j0.8602	53.05	G1–G5, DFIG, PV

Partial eigenvalues based on the above three operating conditions when the transmission distance is 50 km and 100 km are shown in Table 4 and Table 5, respectively. From Table 4 and

Table 5, we can get the same conclusion that combining the PSS and SSSC gives better damping characteristics than using the PSS alone.

Table 4. Partial eigenvalues of the system when the transmission distance is 50 km

Case	Mode	Eigenvalue (λ)	Damping ratio (ζ) [%]	Related units
Case 1	1	–0.8593 ± j6.0243	14.12	G1 G2
	2	–1.3430 ± j7.1041	18.58	G3 G4
	3	–1.0161 ± j5.1556	19.34	G2 G5
	4	–0.4050 ± j3.5421	11.36	G3–G5
	5	–0.3743 ± j0.8347	40.92	G1–G5, DFIG, PV
Case 2	1	–2.1718 ± j6.2747	32.71	G1 G2
	2	–3.3603 ± j8.8282	35.57	G3 G4
	3	–1.0385 ± j4.5839	22.10	G2 G5
	4	–0.7421 ± j3.3698	21.51	G3–G5
	5	–0.5871 ± j0.8631	56.24	G1–G5, DFIG, PV
Case 3	1	–2.2247 ± j6.3274	33.17	G1 G2
	2	–3.3743 ± j8.8178	35.74	G3 G4
	3	–1.3532 ± j4.6556	27.91	G2 G5
	4	–0.8437 ± j3.3670	24.31	G3-G5
	5	–0.5824 ± j0.8116	58.30	G1–G5, DFIG, PV

Assume that a three-phase short-circuit fault occurs at the double-circuit line 8–9 of the interconnected system at 1.0 s and that the fault lasts for 0.05 s. The frequency is 60 Hz. The simulation time is set as 15 s. The time-domain simulation of V_{bus14} and P_{G1} based on the above three operating conditions when the transmission distance is 200 km is shown in Fig. 5. When

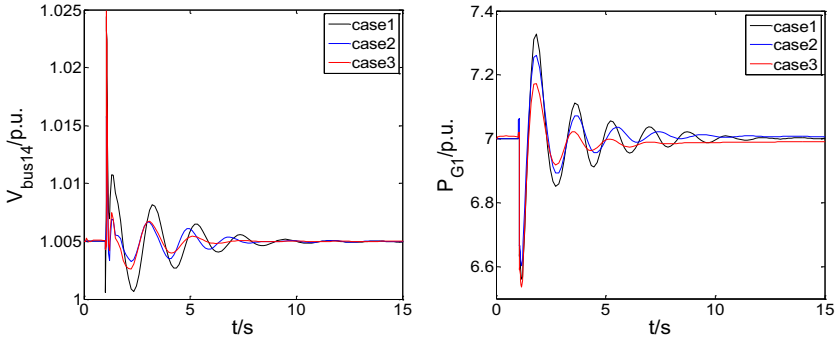

(a) (b)

Fig. 5. Three-phase short-circuit response curves when the transmission distance is 200 km

Table 5. Partial eigenvalues of the system when the transmission distance is 100 km

Case	Mode	Eigenvalue (λ)	Damping ratio (ζ) [%]	Related units
Case 1	1	–0.8603 ± j5.9612	14.28	G1 G2
	2	–1.3399 ± j7.1056	18.53	G3 G4
	3	–0.6690 ± j4.6065	14.37	G2 G5
	4	–0.3910 ± j3.4184	11.36	G3–G5
	5	–0.3720 ± j0.8868	38.68	G1–G5, DFIG, PV
Case 2	1	–2.1145 ± j6.2169	32.20	G1 G2
	2	–3.3445 ± j8.8391	35.39	G3 G4
	3	–0.8878 ± j4.1916	20.72	G2 G5
	4	–0.6259 ± j3.2464	18.93	G3–G5
	5	–0.5392 ± j0.8413	53.96	G1–G5, DFIG, PV
Case 3	1	–2.1906 ± j6.2840	32.92	G1 G2
	2	–3.3724 ± j8.8186	35.72	G3 G4
	3	–1.1005 ± j4.3120	24.73	G2 G5
	4	–0.7852 ± j3.2385	23.56	G3–G5
	5	–0.5862 ± j0.8221	58.06	G1–G5, DFIG, PV

a damper controller is not added, the oscillation curves of V_{bus14} and P_{G1} can still converge, but the convergence speed is relatively slow in case 1. The convergence rate is faster but the oscillation duration is still relatively long when only the PSS is integrated in case 2. Moreover, the convergence rate is obviously the fastest in case 3 when the PSS and SSSC are both integrated into the system. In other words, the system can quickly enter a stable state after a short period of oscillation when a large disturbance occurs due to the interaction of the PSS and SSSC.

4.3. Effect of capacity proportion of wind-PV and thermal power

This section mainly focuses on the influence of a PSS and SSSC on the damping characteristics for a set capacity proportion of wind-PV and thermal power (the ratio of the total grid-connected capacity of wind power and photovoltaic power to that of thermal power) in the wind-PV-thermal-bundled power transmission system. The capacity proportion of wind-PV and thermal power remains 1:3 in the three operating conditions.

Partial eigenvalues based on the above three operating conditions are shown in Table 6. As seen directly from Table 6, the damping ratios of case 1, when there is no damping device, are the smallest. There is a clear upward trend in the damping ratios of case 2 when only the PSS is integrated. In addition, the system has the best damping ratios in case 3 when the PSS and SSSC are both integrated into the system. As a result, we can easily conclude that combining the PSS and SSSC is superior to using the PSS only in improving the system damping.

Table 6. Partial eigenvalues of the system when the capacity proportion of wind-PV and thermal power remains 1:3

Case	Mode	Eigenvalue (λ)	Damping ratio (ζ) [%]	Related units
Case 1	1	–0.8728 ± j6.0514	14.28	G1 G2
	2	–1.3344 ± j7.1106	18.44	G3 G4
	3	–1.0530 ± j5.1191	20.15	G2 G5
	4	–0.4197 ± j3.5624	11.70	G3–G5
	5	–0.3426 ± j0.9188	34.94	G1–G5, DFIG, PV
Case 2	1	–2.2640 ± j6.3915	33.39	G1 G2
	2	–3.3656 ± j8.8261	35.63	G3 G4
	3	–1.4124 ± j5.1585	26.41	G2 G5
	4	–0.8141 ± j3.4788	22.79	G3–G5
	5	–0.5265 ± j0.8708	51.74	G1–G5, DFIG, PV
Case 3	1	–2.2880 ± j6.4359	33.50	G1 G2
	2	–3.3694 ± j8.8230	35.68	G3 G4
	3	–1.8879 ± j5.3056	33.52	G2 G5
	4	–0.8783 ± j3.4830	24.45	G3–G5
	5	–0.5387 ± j0.8420	53.89	G1–G5, DFIG, PV

The time-domain simulation of V_{bus14} and P_{G2} based on the above three operating conditions when the capacity proportion of wind-PV and thermal power remains 1:3 is shown in Fig. 6. We find that the curve of V_{bus14} and P_{G2} continues to oscillate for a long time before it finally converges

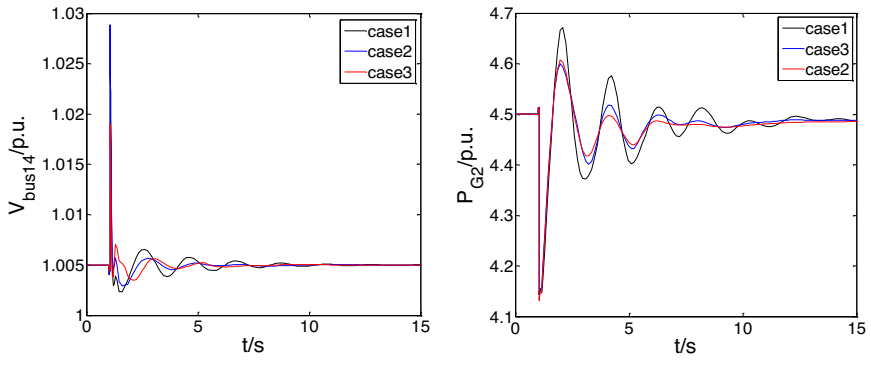

(a) (b)

Fig. 6. Three-phase short-circuit response curves when the capacity proportion of wind-PV and thermal power remains 1:3

in case 1 when a damper controller is not added. The oscillation time is slightly shortened but the convergence rate is still relatively slow in case 2 when only the PSS is integrated. Moreover, the convergence rate is distinctly the fastest in case 3 when the PSS and SSSC are both integrated into the system. Overall, the system can quickly enter a stable state after a short period of oscillation under the action of the PSS and SSSC when a large disturbance occurs.

4.4. Effect of AC/DC transmission power ratio

In fact, the power transmission ratio of AC/DC lines can be adjusted by changing the transmission power of the DC line. And the power transmission ratio of AC/DC lines is inversely related to the small-signal stability of the power system. More accurately, the power system can obtain better damping characteristics by reducing the power transmission ratio of AC/DC lines properly.

The influence of a PSS and SSSC on the damping characteristics for a set AC/DC transmission power ratio in the wind-PV-thermal-bundled power transmission system is intensively studied in this section. The AC/DC transmission power ratio remains 1:3 in the three operating conditions.

Partial eigenvalues based on the above three operating conditions are shown in Table 7. From Table 7, as mentioned above, we can clearly see that the damping ratios of case 1 are relatively small when a damping device is not added. A marked improvement occurs for the damping ratios of case 2 because of the integration of the PSS. Moreover, the system has the highest damping

Table 7. Partial eigenvalues of the system when the AC/DC transmission power ratio remains 1:3

Case	Mode	Eigenvalue (λ)	Damping ratio (ζ) [%]	Related units
Case 1	1	–0.8561 ± j5.9277	14.29	G1 G2
	2	–1.3026 ± j7.1306	17.97	G3 G4
	3	–0.5356 ± j4.1671	12.75	G2 G5
	4	–0.3827 ± j3.3020	11.51	G3–G5
	5	–0.3672 ± j0.8570	39.38	G1–G5, DFIG, PV
Case 2	1	–2.0845 ± j6.1290	31.91	G1 G2
	2	–3.3246 ± j8.8527	35.16	G3 G4
	3	–0.9114 ± j4.1413	21.49	G2 G5
	4	–0.6211 ± j3.2576	18.73	G3–G5
	5	–0.5814 ± j0.8017	58.71	G1–G5, DFIG, PV
Case 3	1	–2.0775 ± j6.2737	32.79	G1 G2
	2	–3.3715 ± j8.8189	35.71	G3 G4
	3	–1.1108 ± j4.3689	24.64	G2 G5
	4	–0.7819 ± j3.2648	23.29	G3–G5
	5	–0.5935 ± j0.8109	59.06	G1–G5, DFIG, PV

ratios in case 3 under the interaction of the PSS and SSSC. Therefore, the above analysis proves that the combination of the PSS and SSSC better improves the system damping.

The time-domain simulation of V_{bus14} and P_{G1} based on the above three operating conditions while the AC/DC transmission power ratio remains 1 : 3 is shown in Fig. 7. Comparing the curves of V_{bus14} and P_{G1}, when a damper controller is not added, the curves of case 1 can converge in the end after a series of long-time oscillations. The sustained oscillation time becomes shorter to a certain extent, but the convergence rate is still relatively slow, when only the PSS is used in case 2. The convergence rate is evidently the fastest in case 3 when both the PSS and SSSC are used. In brief, the disturbance is effectively suppressed, and the oscillation is soon eliminated as a result of the combination of the PSS and SSSC.

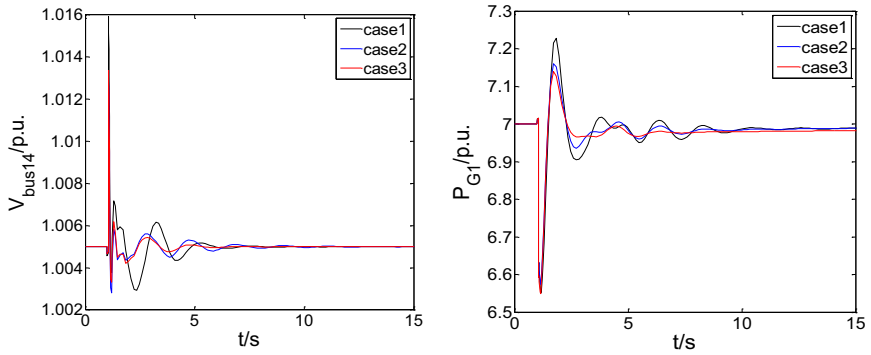

(a) (b)

Fig. 7. Three-phase short-circuit response curves when the AC/DC transmission power ratio remains 1:3

The influence of other operating conditions on the damping characteristics of the wind-PV-thermal-bundled power transmission system, for example, the electrical distance among wind power, photovoltaic power and thermal power (the distance between the thermal power units, wind power units, photovoltaic power stations and bus 12 in the sending system in Fig. 4) as well as the wind power, PV power and thermal power capacities, is not discussed here. Just as important as the previous results, the effect of the PSS and SSSC are basically identical for the various operating conditions; that is, the PSS and SSSC can enhance the damping characteristics of each oscillation mode, accelerate the convergence speed after a large disturbance, and improve the static and dynamic stability of the system.

5. Index – gain rate

To study the effect of a PSS and SSSC on improving the damping characteristics, an index named the gain rate (K) is defined to measure the improvement of the stability limitations of various wind-PV-thermal operating conditions with the PSS and SSSC. It is noteworthy that the range of K is $[0, +\infty]$. In addition, the larger K is, the better the effect of the PSS and SSSC on

improving the damping characteristics of the system.

$$K = \frac{\text{limitation}_{\text{with PSS and SSSC}} - \text{limitation}_{\text{without PSS and SSSC}}}{\text{limitation}_{\text{without PSS and SSSC}}} . \tag{8}$$

The gain rates of various wind-PV-thermal operating conditions are shown in Table 8. We can find that, except for the thermal power capacity, significant improvements of the stability limitations occur for the other various wind-PV-thermal operating conditions. The reason for this result is probably that the PSS and SSSC can dramatically adjust the transmission power and effectively suppress low frequency oscillations by increasing the damping torque and changing the impedance of the transmission line.

Taking the electrical distance among wind, PV and thermal power as an example, the time-domain simulation of V_{bus14} and P_{G1} based on case 1 and case 3 when the electrical distance is set as 300 km is shown in Fig. 8. The curves in case 1 maintain a state of continuous oscillation divergence, while the curves in case 3 rapidly stabilize after a short period of fluctuation when suffering a large disturbance.

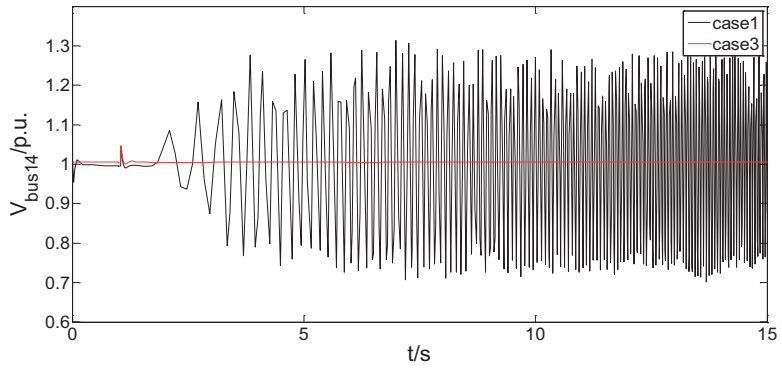

(a)

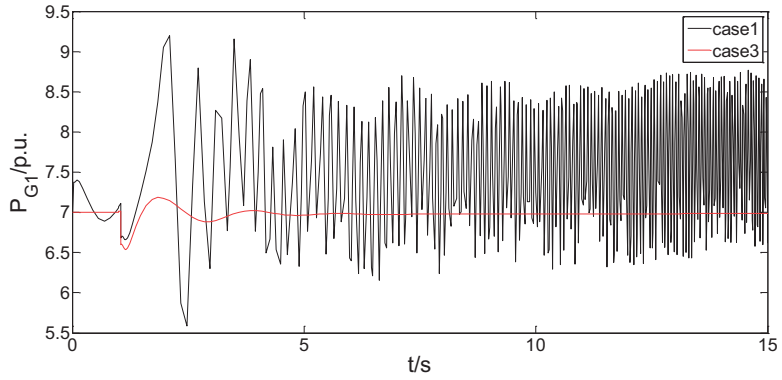

(b)

Fig. 8. Three-phase short-circuit response curves when the electrical distance among wind PV and thermal power is 300 km

Table 8. Gain rates under various wind-PV-thermal operating conditions

	Transmission distance	**Electrical distance among wind, PV and thermal power**	**Wind power capacity**	**PV power capacity**	**Thermal power capacity**	**Capacity ratio of wind, PV and thermal power**	**AC/DC transmission power ratio**
Without PSS or SSSC	200 km	200 km	70 MW	100 MW	600 MW	1:3	1:8
With PSS and SSSC	250 km	300 km	75 MW	130 MW	600 MW	1:3.5	1:12
Gain rate *K*	25%	50%	7.14%	33.3%	0%	16.67%	50%

6. Conclusions

The large-scale integration of wind and solar energy will make the system extremely vulnerable to low frequency oscillations when disturbed due to the decrease of damping. Based on this undesirable situation, this paper is devoted to improving the damping characteristics and dynamic stability of wind-PV-thermal-bundled power transmission systems by combining PSS and SSSC under various wind-PV-thermal operating conditions. In addition, an index-gain rate is defined to demonstrate the improvement of the stability limitations of various wind-PV-thermal operating conditions with PSS and SSSC. Finally, the following conclusions can be drawn through eigenvalue analysis and time-domain simulation:

1. PSS can indeed improve the damping of low frequency oscillations and accelerate the stabilization of oscillations to a certain extent. The oscillation time, however, is still relatively long.
2. Combining PSS and SSSC gives better damping characteristics for a wind-PV-thermal-bundled power transmission system. Moreover, the system can quickly enter a stable state after a shorter period of oscillation when a large disturbance occurs. In brief, combining PSS and SSSC is superior to using PSS only in improving the static and dynamic stability of a power system.
3. There are significant increases in the stability limitations of various wind-PV-thermal operating conditions when PSS and SSSC are adopted. The reason for this result is probably that PSS and SSSC can dramatically adjust the transmission power and effectively suppress low frequency oscillations by increasing the damping torque and changing the impedance of the transmission line.

Acknowledgements

The authors gratefully acknowledge the research funding provided by the National Natural Science Foundation of China (NSFC) (No.51507157, No.51607158), and Technological Research Foundation of

Henan Province (No. 202102210305), and the Project for University Key Teachers of Henan Province (2017GGJS093).

References

[1] Ackermann T., *Wind power in power systems*, Chichester: John Wiley and Sons, pp. 1–30 (2005).

[2] Xiao H.W., Du W.J., Wang H.F., *A Case Study of wind-PV-thermal-bundled AC/DC power transmission from a weak AC network*, Asia Conference on Power and Electrical Engineering (ACPEE), vol. 199, no. 1 (2013).

[3] Chen Y., Chen D.Z., Wang Y., *Studies on high-frequency generator tripping strategy for sending system of wind-PV-thermal-bundled power transmitted by HVDC*, International Conference on Renewable Power Generation (RPG), vol. 2015, no. CP679 (2015).

[4] Chen Y., Chen D.Z., Ma S.Y., *Studies on high-frequency generator tripping strategy for wind-photovoltaic-thermal bundled power transmitted by AC/DC system*, Power System Technology, vol. 40, no. 1, pp. 186–192 (2016).

[5] He P., Wen F.S., Ledwich G., *An investigation on inter-area mode oscillations of interconnected power systems with integrated wind farms*, International Journal of Electrical Power and Energy Systems, vol. 78, no. 2, pp. 145–157 (2016).

[6] Mohseni-Bonab S.M., Rabiee A., *Optimal reactive power dispatch: a review, and a new stochastic voltage stability constrained multi-objective model at the presence of uncertain wind power generation*, IET Generation, Transmission and Distribution, vol. 11, no. 4, pp. 815–829 (2017).

[7] Du W.J., Bi J.T., Wang T., *Impact of grid connection of large-scale wind farms on power system small-signal angular stability*, Chinese Society for Electrical Engineering Journal of Power and Energy Systems, vol. 1, no. 2, pp. 83–89 (2015).

[8] Du W.J., Bi J.T., Cao J., *A Method to Examine the Impact of Grid Connection of the DFIGs on Power System Electromechanical Oscillation Modes*, IEEE Transactions on Power Systems, vol. 31, no. 5, pp. 3775–3784 (2016).

[9] Remon D., Cantarellas A.M., Mauricio J.M., *Power system stability analysis under increasing penetration of photovoltaic power plants with synchronous power controllers*, IET Renewable Power Generation, vol. 11, no. 06, pp. 733–741 (2017).

[10] Remon D., Cañizares C.A., Rodriguez P., *Impact of 100-MW-scale PV plants with synchronous power controllers on power system stability in northern Chile*, IET Generation, Transmission and Distribution, vol. 11, no. 11, pp. 2958–2964 (2017).

[11] Eftekharnejad S., Vittal V., Heydt G.T., *Small stability assessment of power systems with increased penetration of photovoltaic generation: a case study*, IEEE Transactions on Power Systems, vol. 4, no. 4, pp. 960–967 (2013).

[12] Eftekharnejad S., Vittal V., Heydt G.T., *Impact of increased penetration of photovoltaic generation on power systems*, IEEE Transactions on Power Systems, vol. 28, no. 2, pp. 893–901 (2013).

[13] Kulkarni N., Kamalasadan S., Ghosh S., *An integrated method for optimal placement and tuning of a power system stabilizer based on full controllability index and generator participation*, IEEE Transactions on Industry Applications, vol. 51, no. 5, pp. 4201–4211 (2015).

[14] Talha A., Qureshi I.S., *Small signal stability analysis of power system with wind generation using optimized wind PSS*, Saudi Arabia Smart Grid (SASG), Jeddah, pp. 1–5 (2015).

[15] Bhukya J., Mahajan V., *Mathematical modelling and stability analysis of PSS for damping LFOs of wind power system*, IET Renewable Power Generation, vol. 13, no. 1, pp. 103–115 (2019).

[16] Kahouli O., Jebali M., Alshammari B., *PSS design for damping low-frequency oscillations in a multi-machine power system with penetration of renewable power generations*, IET Renewable Power Generation, vol. 13, no. 1, pp. 116–127 (2019).

[17] Bian X.Y., Geng Y., Lo K.L., *Coordination of PSSs and SVC damping controller to improve probabilistic small-signal stability of power system with wind farm integration*, IEEE Transactions on Power Systems, vol. 31, no. 3, pp. 2371–2382 (2016).

[18] Sahraei-Ardakani M., Hedman K.W., *Computationally efficient adjustment of FACTS set points in DC optimal power flow with shift factor structure*, IEEE Transactions on Power Systems, vol. 32, no. 3, pp. 1733–1740 (2017).

[19] Zhang X.H., Shi D., Wang Z.W., *Optimal allocation of series FACTS devices under high penetration of wind power within a market environment*, IEEE Transactions on Power Systems, vol. 33, no. 6, pp. 6206–6217 (2018).

[20] Kapetanaki A., Levi V., Buhari M., *Maximization of wind energy utilization through corrective scheduling and FACTS deployment*, IEEE Transactions on Power Systems, vol. 32, no. 6, pp. 4764–4773 (2017).

[21] Wang L., Ke S.C., Prokhorov A.V., *Stability and power-flow control of a multi-machine power system connected with a hybrid offshore wind farm using a unified power-flow controller*, IEEE/IAS 52nd Industrial and Commercial Power Systems Technical Conference (I&CPS), Detroit, MI, pp. 1−8 (2016).

[22] Rajaram T., Reddy J.M., Xu Y.J., *Kalman filter based detection and mitigation of sub-synchronous resonance with SSSC*, IEEE Transactions on Power Systems, vol. 32, no. 2, pp. 1400–1409 (2017).

[23] Jowder F.A.L., *Influence of mode of operation of the SSSC on the small disturbance and transient stability of a radial power system*, IEEE Transactions on Power Systems, vol. 20, no. 2, pp. 935−942 (2005).

[24] Pillai G.N., Ghosh A., Joshi A., *Torsional interaction between an SSSC and a PSS in a series compensated power system*, in IEE Proceedings – Generation, Transmission and Distribution, vol. 149, no. 6, pp. 653–658 (2002).

[25] Kumar R., Sahu B., Shiva C.K., Rajender B., *A control topology for frequency regulation capability in a grid integrated PV system*, Archives of Electrical Engineering, vol. 69, no. 2, pp. 389–401 (2020).

[26] Jayalakshmi N.S., Gaonkar D.N., Karthik R.P., Prasanna P., *Intermittent power smoothing control for grid connected hybrid wind/PV system using battery-EDLC storage devices*, Archives of Electrical Engineering, vol. 69, no. 2, pp. 433–453 (2020).

[27] Bian X.Y., Geng Y., Lo K.L., *Coordination of PSSs and SVC damping controller to improve probabilistic small-signal stability of power system with wind farm integration*, IEEE Transactions on Power Systems, vol. 31, no. 3, pp. 2371–2382 (2016).

[28] He P., Wen F.S., Ledwich G., *Effects of various power system stabilizers on improving power system dynamic performance*, International Journal of Electrical Power and Energy Systems, vol. 46, no. 1, pp. 175–183 (2013).

[29] Farahani M., *Damping of subsynchronous oscillations in power system using static synchronous series compensator*, IET Generation, Transmission and Distribution, vol. 6, no. 6, pp. 539–544 (2012).

[30] Benabid R., Boudour M., Abido M.A., *Development of a new power injection model with embedded multi-control functions for static synchronous series compensator*, IET Generation, Transmission and Distribution, vol. 6, no. 7, pp. 680–692 (2012).